RSC Advances

PAPER

View Article Online
View Journal | View Issue

Cite this: *RSC Adv.*, 2021, **11**, 35046

Broadband saturated absorption properties of bismuthene nanosheets

Yan Sun, †* Junjie Yuan,† Yi Xin,† Guowei Liu,† Fang Zhang, Fei Xing and Shenggui Fu

The nonlinear absorption properties of two-dimensional bismuthene nanosheets have great value for application in the photonics field. In this work, bismuthene nanosheets with a thickness of around 4 nm were prepared using the liquid phase exfoliation (LPE) method. The infrared waveband nonlinear absorption properties of bismuthene nanosheets were investigated using the open aperture Z-scan technique with four wavelengths of 950, 1064, 1200, and 1500 nm, respectively. Bismuthene nanosheets exhibited broadband saturated absorption (SA) properties at the infrared band. The lower saturated intensity indicated the advantages of bismuthene as a saturated absorber in the application of ultra-fast lasers in the infrared band.

Received 10th August 2021
Accepted 21st October 2021

DOI: 10.1039/d1ra06046e

rsc.li/rsc-advances

1 Introduction

In the past two decades, two-dimensional (2D) layered materials were a hot research area due to their unique electronic structures and abundant surface atoms since the discovery of graphene.[1] The special structure and quantum confinement effect endow them with unique optoelectronic properties, such as significantly different nonlinear optical behaviors.[2–4] Antimonene, first discovered in 2015 with high stability and carrier mobility, can be widely used in electrocatalysis, energy storage, and optical devices.[5–9] In 2017, Lu *et al.* first discovered the strong nonlinear optical response of antimonene in the visible light band, which promoted the application of antimonene in nonlinear optical devices and other fields.[10] Wang *et al.* employed antimonene in Er- and Tm-doped fiber lasers to realize ultrafast lasers with mode-locked pulse output.[11] Recently, owing to copious applications in optoelectronics, there is a growing interest for low-dimensional materials with second and third order nonlinearities such as few-layer graphene,[12] 2D graphdiyne,[13] MoS_2 nanoflakes,[14] semi-organic single-crystal,[15] metallic oxide thin film,[16,17] low-dimensional material from bismuth oxyhalide[18] and so on. Shinji Yamashita focused on the nonlinear optical properties of graphene and carbon nanotube to further their superior application value in fiber lasers, modulators, and other fields.[19] Zhang *et al.* discovered the broadband Kerr nonlinear effect of 2D graphdiyne and revealed its important application value in photonic diodes.[20] R. I. Woodward *et al.* devoted to research the second- and third-order nonlinear of monolayer MoS_2, highlighting the potential for telecommunications.[21] And more than dozens of MOFs have been discovered and their unique properties are gradually being revealed and unearthed.[22–24]

As a group-VA elemental material, bismuth (Bi) received tremendous interests owing to its advantages in electronic-transport and semi-metallic bonding.[25,26] When the dimension is lowered down to the nano-scale level, the transition from semi-metal to semi-conductor occurs because of the quantum confinement effect, which makes low-dimensional bismuth holding promising application potential in the fields of Q-switcher,[27] electrode,[28,29] energy storage[30] and optoelectronic devices[31] *etc.* Bismuth nanorod[32] displayed excellent optical limiting properties at both 532 and 1064 nm excitations. Bismuth nanospheres[33] presented obvious nonlinear refraction properties under 800 nm excitations. In 2005, Tomoharu Hasegawa *et al.* explored the third-order optical nonlinearities in bismuth-based glasses through the Z-scan technique and found excellent nonlinear optical behaviors, which can promote the application of bismuth in nonlinear devices.[34] E. M. Dianov *et al.* have realized the development and application of bismuth-doped fiber laser, value in the field of fiber photonics.[35] What's more, Bismuth also has important applications in the fields of plasmonics, nanophotonics, and magnetooptics.[36,37] However, there is little research on the nonlinear absorption properties of bismuth in the broadband near-infrared band, which gives us new research directions and inspirations.

In fundamental research's foundation of pure Bi material, this work investigated the nonlinear absorption responses of 2D bismuthene nanosheets using Z-scan technique from 950 nm to 1500 nm wavelengths, which will provide new insights for nonlinear photonic devices and promote its application in near-infrared ultrafast lasers.

School of Physics and Optoelectronic Engineering, Shandong University of Technology, Zibo 255000, China. E-mail: sunyan19802012@163.com

† These authors contribute equally to this work.

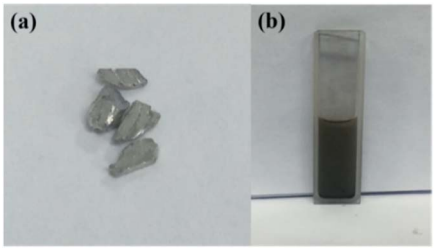

Fig. 1 (a) Bismuth crystal, (b) Prepared bismuthene dispersion liquid.

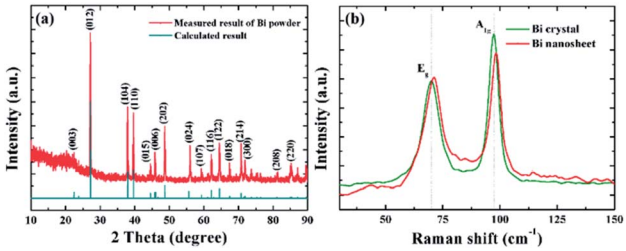

Fig. 3 (a) Measured and calculated XRD results of bismuth powders, (b) Raman spectrum of Bi crystal and bismuthene nanosheets.

2 Experimental section

2.1 Sample preparation

Bismuthene nanosheets were prepared by the LPE method. Bismuth crystal (Fig. 1(a)) with 100 mg was ground for about 5 hours to peel off with the participation of absolute ethanol. The nanosheets were dispersed using 40 kHz ultrasonic wave in the dispersion liquid for about 1.5 hours. And then the dispersion was centrifuged for 30 minutes. One fifth of the upper dispersion liquid was collected for the nonlinear absorption measurement and the sample characterization. Hereto, the bismuthene dispersion liquid has been prepared successfully, which is shown in Fig. 1(b).

2.2 Characterization

Scanning electron microscope (SEM) was employed to detect the morphology characteristics of bismuth crystal and bismuthene nanosheets. Fig. 2(a) shows the SEM image of bismuth crystal. It can be seen that bismuth crystal possesses apparent layer structure, which indicates that bismuth can be exfoliated easily by LPE or other exfoliation method. Fig. 2(b) gives the SEM image of exfoliated bismuthene nanosheets. Bismuthene nanosheets display two-dimensional layer structure, and there are apparent stratified structures at the edge, which are marked by red circles. The thicknesses of bismuthene nanosheets are measured by atomic force microscopy (AFM) shown in Fig. 2(c). The corresponding heights of line 1, 2 are given in Fig. 2(d). As shown, the heights of bismuthene nanosheets are around 4 nm.

X-ray diffraction (XRD) measurements were used to detect the crystalline of the bismuth powders, which is shown in Fig. 3(a). The characteristic peaks of 2 theta at 22.467°, 27.165°, 37.949°, 39.618°, 44.553°, 45.872°, 48.689°, 55.640°, 59.324°, 62.174°, 64.496°, 67.443°, 70.764°, 71.865°, 81.145° and 85.320° correspond to the crystallographic plane of (003), (012), (104), (110), (015), (006), (202), (024), (107), (116), (122), (018), (214), (300), (208) and (220). The XRD patterns of the measured results of Bi powder match well with that of calculated results and can be indexed to be hexagonal rhomb-centered phase of bismuth.[38–40] In order to explore the structural characterization of samples further, Raman spectra was measured. The characteristic peaks of Bi crystal and bismuthene nanosheet are shown in the Fig. 3(b). Two peaks at E_g (71.17 cm^{-1}) and A_{1g} (98.35 cm^{-1}) belongs to the in-plane vibration and out-of-plane vibration modes of bismuthene nanosheet[41]. The vibrational modes of bismuthene nanosheet of E_g and A_{1g} show slight blue shifts comparing to that of Bi crystal, which indicates the nanosheets are effectively exfoliated.

Fig. 4 gives the relationship between linear transmittance and wavelengths of prepared bismuthene nanosheets, which was detected by ultraviolet-visible-nearinfrared spectrophotometer. The effects of alcohol and quartz cell have been eliminated. The peaks around 950 and 1500 nm forebode weak absorption. The transmittances at 950, 1064, 1200 and 1500 nm are 59.5%, 53.1%, 52.8% and 55.0%, respectively. According to the equation $T_0 = \exp(-\alpha_0 l)$, where T_0 is linear transmittance

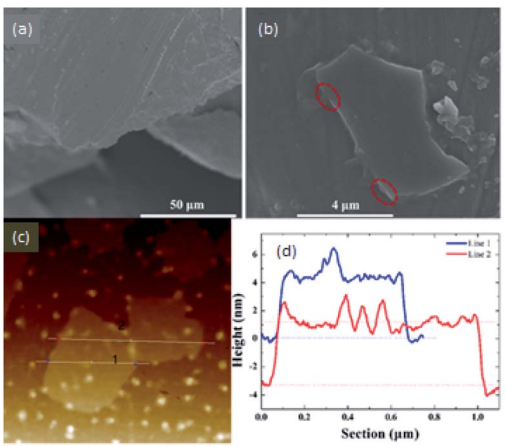

Fig. 2 SEM images of (a) bismuth crystal, (b) bismuthene nanosheets, (c) AFM of bismuthene nanosheets and (d) corresponding heights of trances 1, 2.

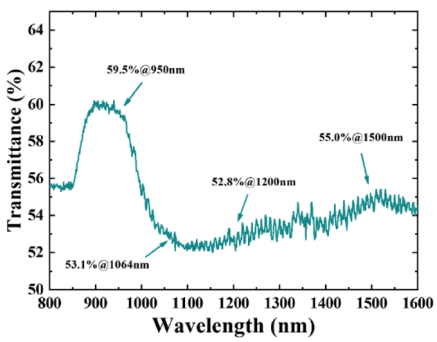

Fig. 4 Relationship between linear transmittance and wavelength.

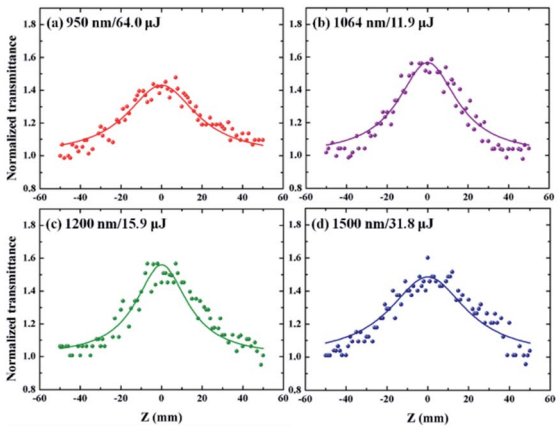

Fig. 5 Experimental (points) and fitting (solid lines) results of open-aperture Z-scan curves of bismuthene nanosheets at different wavelengths.

and $l = 2$ mm is the thickness of the sample interact with the laser, the linear absorption coefficients α_0 can be calculated to be 2.60, 3.16, 3.19, 2.99 cm^{-1} at 950, 1064, 1200 and 1500 nm wavelengths, respectively.

2.3 NLA properties of bismuthene nanosheets

The nonlinear absorption properties of bismuthene nanosheets were measured by open aperture Z-scan technique using nanosecond laser. The pulse duration and repetition rate are 6 ns and 10 Hz, respectively.

Fig. 5 shows the Z-scan results for bismuthene nanosheets with different pulse energies and four wavelengths at 950, 1064, 1200, 1500 nm, respectively. A peak of wave can be observed at the largest point of energy density ($Z = 0$) at each wavelength. With the increasing of excited intensity, the increasing transmittance manifests the apparent saturated absorption properties of bismuthene nanosheets at the four excited wavelengths mentioned above. When the excited wavelengths were 950, 1064, 1200, 1500 nm and intensities were 64.0, 11.9, 15.9, and 31.8 μJ, respectively, the maximum normalized transmittances of wave peaks were 143%, 157%, 155%, and 148%, corresponding to the normalized modulation depth of 43%, 57%, 55%, 48% at four wavelengths. The lower excited intensity and larger modulation depth at 1064 and 1200 nm wavelengths imply much more superior nonlinear absorption properties, comparing to other wavelengths at 950 and 1500 nm wavelengths.

Fig. 6 gives the variations of normalized transmittance with excited energy density at four excited wavelengths. The results exhibited that 2D bismuthine nanosheets owned a lower nonlinear threshold at 1064 and 1200 nm, which is consistent with the experimental results in Fig. 5, implying the great potential of bismuthene as a saturable absorber in these wavebands.

3. Results and discussion

The nonlinear absorption theory based on Z-scan is expressed by following eqn (1):

$$T = \frac{1 - \alpha(I)l}{1 - \alpha_0 l} \quad (1)$$

where T is normalized transmittance, and α_0 is the linear absorption coefficient. With the saturated absorption part is solely considered, the $\alpha(I)$ can be expressed as follows:

$$\alpha(I) = \frac{\alpha_0}{1 + I(z)/I_s} \quad (2)$$

where I_s is the saturable intensity. $I(z) = I_0/(1 + z^2/{z_0}^2)$ is the power density at z-position of sample, I_0 is the peak power density at $z = 0$ and z_0 is the Rayleigh length. The normalized transmittance can be expressed as eqn (3):

$$T = \left[1 - \frac{\alpha_0 I_s l}{I_s + I_0/(1 + z^2/{z_0}^2)}\right] \Big/ (1 - \alpha_0 L) \quad (3)$$

Using eqn (3), the saturable intensity I_s with different wavelengths were calculated. Fig. 7 shows the relationship between I_s and wavelengths. The I_s at 950, 1064, 1200 and 1500 nm with excited intensities of 64.0, 11.9, 15.9 and 31.8 μJ were 105 ± 3, 26 ± 1, 37 ± 2 and 38±1 MW cm^{-2}, respectively. The I_s at 1064 nm was the lowest and the I_s at 950 nm was the largest. The reason may be the different absorption intensities at different wavelengths, which could be reflected in the linear transmittance spectrum (Fig. 4). A strong peak in Fig. 4 around 950 nm indicated the weak absorption and the slight trough around 1064 nm implied the strong absorption. Analogously, the nonlinear results at 1200 and 1500 nm wavelengths exhibited similar properties. In addition, the linear and

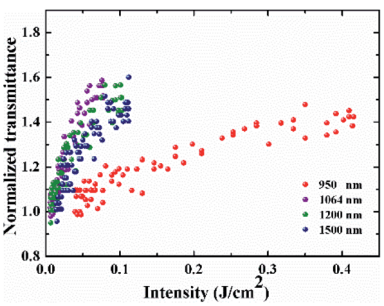

Fig. 6 Relationship of normalized transmittance with excited energy density of bismuthene nanosheets with four excited wavelengths.

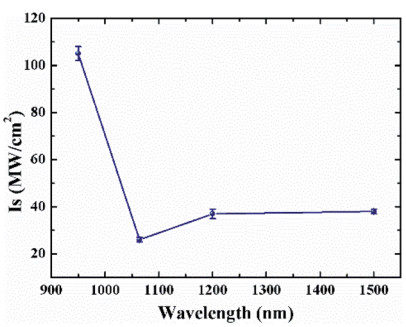

Fig. 7 Relationship between saturable intensity and wavelength.

Table 1 Linear and nonlinear absorption coefficients at different wavelengthsof bismuthine nanosheets

Wavelength (nm)	T (%)	α_0 (cm^{-1})	Modulation depth	I_s (MW cm^{-2})
950	59.5	2.60	43%@64.0 μJ	105 ± 3
1064	53.1	3.16	57%@11.9 μJ	26 ± 1
1200	52.8	3.19	55%@15.9 μJ	37 ± 2
1500	55.0	2.99	48%@31.8 μJ	38 ± 1

nonlinear absorption results of bismuthene nanosheets were generalized in Table 1. In a word, our results demonstrated the excellent and broadband saturated absorption properties of bismuthene nanosheets, which will provide guidance for the application of bismuthene in the ultrafast and high-energy laser field.

4. Conclusions

In summary, we successfully exfoliated the bismuthene nanosheets using liquid phase exfoliation (LPE) method. And the saturated absorption properties at 950, 1064, 1200, 1500 nm have been studied by open aperture Z-scan method. The results demonstrated that bismuthene nanosheets display excellent and broadband saturated properties in near-infrared wavelengths, especially for 1064 and 1200 nm wavelengths. The lower saturation absorption coefficient at 1064 and 1200 nm also implyed bismuthene nanosheets have great potential application in nonlinear optics, especially in infrared wavelengths. And our research is of great significance for enhancing the application of bismuthene as a saturated saturable absorber in the field of ultrafast lasers in the near-infrared.

Author contributions

Dr Yan Sun wrote the main manuscript. Dr Yan Sun together with Junjie Yuan, Yi Xin, and Guowei Liu did the whole experiment. Prof. Fang Zhang guided the experiment and amended the manuscript text. Dr Fei Xing and Prof. Shenggui Fu provided the technical guidance. All authors discussed the results and commented on the manuscript.

Conflicts of interest

There are no conflicts to declare.

Acknowledgements

This work was supported by the National Natural Science Foundation of China (Grant No. 11704227)

References

1 K. S. Novoselov, A. K. Geim, S. V. Morozov, D. Jiang, Y. Zhang, S. V. Dubonos, I. V. Grigorieva and A. A. Firsov, *science*, 2004, **306**, 666–669.
2 W. Zhang, Q. Wang, Y. Chen, Z. Wang and A. T. Wee, *2D Materials*, 2016, **3**, 022001.
3 J. S. Ponraj, Z.-Q. Xu, S. C. Dhanabalan, H. Mu, Y. Wang, J. Yuan, P. Li, S. Thakur, M. Ashrafi and K. Mccoubrey, *Nanotechnology*, 2016, **27**, 462001.
4 B. T. Hogan, E. Kovalska, M. F. Craciun and A. Baldycheva, *J. Mater. Chem. C*, 2017, **5**, 11185–11195.
5 S. Zhang, Z. Yan, Y. Li, Z. Chen and H. Zeng, *Angew. Chem.*, 2015, **127**, 3155–3158.
6 X. Ren, Z. Li, H. Qiao, W. Liang, H. Liu, F. Zhang, X. Qi, Y. Liu, Z. Huang and D. Zhang, *ACS Appl. Energy Mater.*, 2019, **2**, 4774–4781.
7 V. K. Mariappan, K. Krishnamoorthy, P. Pazhamalai, S. Natarajan, S. Sahoo, S. S. Nardekar and S.-J. Kim, *Nano Energy*, 2020, **77**, 105248.
8 M. M. Ismail, J. Vigneshwaran, S. Arunbalaji, D. Mani, M. Arivanandhan, S. P. Jose and R. Jayavel, *Dalton Trans.*, 2020, **49**, 13717–13725.
9 J. Yuan, G. Liu, Y. Xin, F. Xing, K. Han, W. Zhang, F. Zhang and S. Fu, *Opt. Mater.*, 2021, **118**, 111256.
10 L. Lu, X. Tang, R. Cao, L. Wu, Z. Li, G. Jing, B. Dong, S. Lu, Y. Li and Y. Xiang, *Adv. Opt. Mater.*, 2017, **5**, 1700301.
11 J. Wang, H. Yuan, H. Chen, J. Yin, J. Li, T. He, C. Guo, P. Yan, J. Wang and R. Yang, *J. Lightwave Technol.*, 2020, **38**, 3710–3716.
12 H. Zhang, S. Virally, Q. Bao, L. K. Ping, S. Massar, N. Godbout and P. Kockaert, *Opt. Lett.*, 2012, **37**, 1856–1858.
13 F. Zhang, G. Liu, J. Yuan, Z. Wang, T. Tang, S. Fu, H. Zhang, Z. Man, F. Xing and X. Xu, *Nanoscale*, 2020, **12**, 6243–6249.
14 S. Mirershadi, F. Sattari, A. Alipour and S. Z. Mortazavi, *Frontiers in Physics*, 2020, **8**, 96.
15 R. V. Rajan, M. George, D. Leenaraj, R. Ittyachan, D. Sajan and G. Vinitha, *J. Mol. Struct.*, 2020, **1222**, 128937.
16 G. Ravinder, C. Sreelatha, V. Ganesh, M. Shkir, M. Anis and P. C. Rao, *Mater. Res. Express*, 2019, **6**, 096403.
17 Y. Xu, Y. Lu, Y. Zuo, F. Xu and D. Zuo, *Appl. Opt.*, 2019, **58**, 6112–6117.
18 H. Li, S. Xu, Z. Huang, J. Huang, J. Wang, L. Zhang and C. Zhang, *J. Mater. Chem. C*, 2018, **6**, 8709–8716.
19 S. Yamashita, *APL Photonics*, 2019, **4**, 034301.
20 L. Wu, Y. Dong, J. Zhao, D. Ma, W. Huang, Y. Zhang, Y. Wang, X. Jiang, Y. Xiang and J. Li, *Adv. Mater.*, 2019, **31**, 1807981.
21 R. Woodward, R. Murray, C. Phelan, R. De Oliveira, T. Runcorn, E. Kelleher, S. Li, E. De Oliveira, G. Fechine and G. Eda, *2D Materials*, 2016, **4**, 011006.
22 Y.-H. Xiao, Z.-G. Gu and J. Zhang, *Sci. China: Chem.*, 2020, **63**, 1059–1065.
23 C. Wang, T. Zhang and W. Lin, *Chem. Rev.*, 2012, **112**, 1084–1104.
24 H. He, H. Li, Y. Cui and G. Qian, *Adv. Opt. Mater.*, 2019, **7**, 1900077.
25 C. M. Bedoya Hincapie, M. J. Pinzon Cardenas, J. E. Alfonso Orjuela, E. Restrepo Parra and J. J. Olaya Florez, *Dyna*, 2012, **79**, 139–148.

26 O. V. Kharissova, E. M. Kopnin, V. V. Maltsev, N. I. Leonyuk, L. M. León-Rossano, I. Y. Pinus and B. I. Kharisov, *Crit. Rev. Solid State Mater. Sci.*, 2014, **39**, 253–276.
27 J. Liu, H. Huang, F. Zhang, Z. Zhang, J. Liu, H. Zhang and L. Su, *Photonics Res.*, 2018, **6**, 762–767.
28 X. Hu, D. Pan, M. Lin, H. Han and F. Li, *Microchim. Acta*, 2016, **183**, 855–861.
29 S. Liu, Z. Luo, J. Guo, A. Pan, Z. Cai and S. Liang, *Electrochem. Commun.*, 2017, **81**, 10–13.
30 B. Yang, X. Li, Y. Cheng, S. Duan, B. Zhao, W. Yi, C. Wang, H. Sun, Z. Wang and D. Gu, *J. Mater. Chem. C*, 2020, **8**, 12314–12322.
31 H. Huang, X. Ren, Z. Li, H. Wang, Z. Huang, H. Qiao, P. Tang, J. Zhao, W. Liang and Y. Ge, *Nanotechnology*, 2018, **29**, 235201.
32 S. Sivaramakrishnan, V. S. Muthukumar, S. Sivasankara Sai, K. Venkataramaniah, J. Reppert, A. M. Rao, M. Anija, R. Philip and N. Kuthirummal, *Appl. Phys. Lett.*, 2007, **91**, 093104.
33 C. Yang, Z. Shang, Z. Wang, H. Peng, X. Tang, B. Li and Y. Chen, *J. Opt.*, 2015, **44**, 7–11.
34 T. Hasegawa, T. Nagashima and N. Sugimoto, *Opt. Commun.*, 2005, **250**, 411–415.
35 S. Firstov, S. Alyshev, K. Riumkin, M. Melkumov, O. Medvedkov and E. Dianov, *Opt. Lett.*, 2015, **40**, 4360–4363.
36 J. Toudert, R. Serna, I. n. Camps, J. Wojcik, P. Mascher, E. Rebollar and T. A. Ezquerra, *The Journal of Physical Chemistry C*, 2017, **121**, 3511–3521.
37 G. Scott and D. Lacklison, *IEEE Trans. Magn.*, 1976, **12**, 292–311.
38 J. Zhang, S. Ye, Y. Sun, F. Zhou, J. Song and J. Qu, *Nanoscale*, 2020, **12**, 20945–20951.
39 S. M. Beladi-Mousavi, Y. Ying, J. Plutnar and M. Pumera, *Small*, 2020, **16**, 2002037.
40 J. Zhou, J. Chen, M. Chen, J. Wang, X. Liu, B. Wei, Z. Wang, J. Li, L. Gu and Q. Zhang, *Adv. Mater.*, 2019, **31**, 1807874.
41 E. S. Walker, S. R. Na, D. Jung, S. D. March, J.-S. Kim, T. Trivedi, W. Li, L. Tao, M. L. Lee and K. M. Liechti, *Nano Lett.*, 2016, **16**, 6931–6938.